Regular Article

RED CELLS, IRON, AND ERYTHROPOIESIS

Multiple clinical forms of dehydrated hereditary stomatocytosis arise from mutations in *PIEZO1*

Immacolata Andolfo,[1,2] Seth L. Alper,[3] Lucia De Franceschi,[4] Carla Auriemma,[1,2] Roberta Russo,[1,2] Luigia De Falco,[1,2] Fara Vallefuoco,[1,2] Maria Rosaria Esposito,[1,2] David H. Vandorpe,[3] Boris E. Shmukler,[3] Rupa Narayan,[5] Donatella Montanaro,[1] Maria D'Armiento,[6] Annalisa Vetro,[7] Ivan Limongelli,[7] Orsetta Zuffardi,[7] Bertil E. Glader,[5] Stanley L. Schrier,[8] Carlo Brugnara,[9] Gordon W. Stewart,[10] Jean Delaunay,[11] and Achille Iolascon[1,2]

[1]Department of Molecular Medicine and Medical Biotechnologies, Federico II University of Naples, Naples, Italy; [2]Centro di Ingegneria Genetica (CEINGE), Biotecnologie Avanzate, Naples, Italy; [3]Renal Division and Molecular and Vascular Medicine Division, Beth Israel Deaconess Medical Center and Department of Medicine, Harvard Medical School, Boston, MA; [4]Department of Medicine, University of Verona, Verona, Italy; [5]Division of Hematology-Oncology, Department of Pediatrics, Stanford University School of Medicine, Stanford, CA; [6]Dipartimento di Scienze biomediche avanzate, Federico II University of Naples, Naples, Italy; [7]Department of Molecular Medicine, University of Pavia, Pavia, Italy; [8]Division of Hematology, Department of Medicine, Stanford University School of Medicine, Stanford, CA; [9]Department of Laboratory Medicine, Boston Children's Hospital and Department of Pathology, Harvard Medical School, Boston, MA; [10]Division of Medicine, University College London, London, United Kingdom; and [11]Institut National de la Sante et de la Recherche Médicale (INSERM), Faculté de Médecine Paris-Sud, Université Paris-Sud, Paris, France

Key Points

- Dehydrated hereditary stomatocytosis is characterized by abnormal RBC morphology but may involve pseudohyperkalemia and perinatal edema.
- This syndrome is associated with germline mutations in *PIEZO1*, encoding a transmembrane protein that induces mechanosensitive currents.

Autosomal dominant dehydrated hereditary stomatocytosis (DHSt) usually presents as a compensated hemolytic anemia with macrocytosis and abnormally shaped red blood cells (RBCs). DHSt is part of a pleiotropic syndrome that may also exhibit pseudohyperkalemia and perinatal edema. We identified *PIEZO1* as the disease gene for pleiotropic DHSt in a large kindred by exome sequencing analysis within the previously mapped 16q23-q24 interval. In 26 affected individuals among 7 multigenerational DHSt families with the pleiotropic syndrome, 11 heterozygous *PIEZO1* missense mutations cosegregated with disease. PIEZO1 is expressed in the plasma membranes of RBCs and its messenger RNA, and protein levels increase during in vitro erythroid differentiation of $CD34^+$ cells. PIEZO1 is also expressed in liver and bone marrow during human and mouse development. We suggest for the first time a correlation between a *PIEZO1* mutation and perinatal edema. DHSt patient red cells with the R2456H mutation exhibit increased ion-channel activity. Functional studies of *PIEZO1* mutant R2488Q expressed in *Xenopus* oocytes demonstrated changes in ion-channel activity consistent with the altered cation content of DHSt patient red cells. Our findings provide direct evidence that R2456H and R2488Q mutations in *PIEZO1* alter mechanosensitive channel regulation, leading to increased cation transport in erythroid cells. (*Blood*. 2013; 121(19):3925-3935)

Introduction

Dehydrated hereditary stomatocytosis (DHSt), also known as hereditary xerocytosis (Online Mendelian Inheritance in Man [OMIM] 194380), is an autosomal dominant congenital hemolytic anemia associated with a monovalent cation leak. DHSt consists of a usually compensated hemolysis, associated with moderate splenomegaly.[1,2] Blood smears show variable numbers of stomatocytes, sometimes rare and ill-formed, and likely to be overlooked. The reticulocyte count is elevated, and red cell mean corpuscular volume (MCV) is slightly increased. DHSt red blood cells (RBCs) exhibit decreased intraerythrocytic K^+ content and increased intraerythrocytic Na^+ content, usually accompanied by increased mean corpuscolar hemoglobin (Hb) concentration. The cation leak of DHSt red cells resembles that of control RBCs in its temperature dependence, but is of greater magnitude at all temperatures.[3] The definitive diagnosis of DHSt is ascertained by osmotic gradient ektacytometry, which shows a leftward shift of the bell-shaped curve.[4,5] Occasionally, associated hepatosiderosis beyond that expected from the mild hemolytic state suggests a strong tendency to iron overload.[6] Unlike hereditary spherocytosis, in which splenectomy can be beneficial, splenectomy in DHSt is contraindicated due to increased risk of thromboembolic complications.[7,8]

DHSt can present as an isolated erythroid phenotype or as associated with pseudohyperkalemia, with pre- and/or perinatal edema, or with both pseudohyperkalemia and effusions. The pre- and/or

Submitted February 1, 2013; accepted March 4, 2013. Prepublished online as *Blood* First Edition paper, March 11, 2013; DOI 10.1182/blood-2013-02-482489.

The online version of this article contains a data supplement.

There is an Inside *Blood* commentary on this article in this issue.

The publication costs of this article were defrayed in part by page charge payment. Therefore, and solely to indicate this fact, this article is hereby marked "advertisement" in accordance with 18 USC section 1734.

perinatal edema is of chylous type and may lead to life-threatening hydrops fetalis requiring therapeutic drainage.[9-11] Remarkably, the edema recede spontaneously before birth or within several months postnatally, and do not reappear. In contrast, edema may also be restricted to prenatal, clinically silent ascites detectable only by ultrasound.[12] Isolated familial pseudohyperkalemia (FP) is defined by the time-dependent elevation in serum [K^+] when blood samples are left for several hours or more prior to analysis at temperatures below body temperature, whereas serum [K^+] is normal in freshly drawn blood. FP may be associated with DHSt or, when linked to chromosome 2, as isolated FP. The causative gene of isolated FP linked to 2q35-36 was recently identified as *ABCB6*, encoding a porphyrin transporter.[13]

Mapping of gene(s) responsible for familial DHSt identified a cosegregating critical region at the telomeric region of 16q.[14-17] Zarychanski and colleagues reported for the first time, in 2 families with isolated DHSt, 2 missense mutations in the *FAM38A* gene encoding PIEZO1.[18] We report here our independent findings in 7 unrelated families with isolated DHSt, DHSt with pseudohyperkalemia, or DHSt with both pseudohyperkalemia and pre-/perinatal fluid effusion, novel mutations in the *PIEZO1* gene that cosegregate with the multiple disease phenotypes. We have further characterized PIEZO1 expression in erythroid cells and during mouse and human development, and performed functional studies on R2488Q and R2456H mutations in human erythrocytes and *Xenopus* oocytes.

Material and methods

Case report

The clinical phenotypes of kindreds Arras (AR), Bicêtre (BI), Dax (DA), Essex, and Troyes (TR) were previously described.[14,15] Definitive diagnosis of DHSt was made by ektacytometry. Families Dax and Troyes showed isolated DHSt. Families Arras and Edinburgh showed DHSt plus pseudohyperkalemia.[15,19,20] Family Bicêtre exhibited DHSt accompanied by pseudohyperkalemia and massive perinatal fluid effusions that spontaneously and permanently regressed within several months after birth.[10,15] Similar massive but transient perinatal fluid effusions have been observed by others.[9,11,21,22] Following our initial studies, the patients were followed up locally.

The expressivity of the phenotype was generally similar among members from a given kindred, but some variability was noted. (1) In family Dax, the MCV and ektacytometric curve of the father (II.1; numbering from Grootenboer et al) were only slightly altered, whereas the son (II.2) exhibited a full-fledged DHSt.[15] (2) In family Bicêtre, whereas DHSt in father II.3,[23] was accompanied by pseudohyperkalemia and dramatic perinatal fuid effusions, his 2 children exhibited effusions which were less pronounced. Splenectomy was performed in only 2 patients. In keeping with Stewart et al,[7] member II.2 of family AR[15] developed a thrombosis after a period in an ankle cast, followed some years later by a moderately severe pulmonary embolus, treated by chronic anticoagulation. The second patient, member II.2 of family DA,[15] was without thromboembolic complication at the time of examination.

Patient SF, a 38-year-old female triathlete, has not been reported previously. She was referred by her primary physician to a hematology clinic for evaluation of hemolytic anemia, first diagnosed at age 14 in the setting of severe weakness of 1-month duration. Similar episodes of weakness recurred once in her 20s and again at the age of 32, unrelated to medications or specific foods, and resolving with supportive care. The patient reported chronic "yellowing of her eyes," without changes in color of urine or stool, and without fevers or gastrointestinal symptoms. Neither medication nor food triggered these episodes. Family history was notable for recently diagnosed hemolytic anemia in the patient's brother, accompanied by 50% deficiency of pyruvate kinase, and a report of mild anemia of unclear etiology in the patient's father. Physical examination revealed mild scleral icterus and hepatomegaly (edge 1 cm below costal margin). Hematologic indices were: Hb, 13.2 g/L; hematocrit, 37%; RBCs, 3.57×10^6 mm^3; MCV, 103.7 fL; red cell distribution width, 13.1%; absolute reticulocyte count, 139,300/μL. The peripheral blood smear revealed spherocytes, macrocytes, and rare stomatocytes and tear drops (supplemental Figure 1A-B, available on the *Blood* website; see the supplemental Materials link at the top of the online article). Total bilirubin was 1.4 mg/dL, with normal lactate dehydrogenase, and testing for Gilbert syndrome was negative. Direct Coombs test was negative, and red cell glutathione and enzyme activities (G6PD, PK, GPI, HK, ADA) were normal. Osmotic fragility testing (supplemental Figure 1C) and ektacytometry (supplemental Figure 1D) revealed osmotic resistance, and ektacytometry also showed decreased RBC deformability in hypertonic solutions: hyposmotic point was 112.8 (normal, 139.8 + 16.0 mOsm/kg); maximum deformability index was 0.63 (normal, 0.54 + 0.06 artificial units), osmotic point was 348.7 (normal, 405.6 + 18.3 mosmol/kg). These results supported the clinical diagnosis of dehydrated stomatocytosis (DHSt) in patient SF.

Bioinformatic analysis for exome sequencing

Reads were aligned to the most recent version of human genome (GRCh37/hg19) using the BWA software package (version 0.5.9). Mapped reads were consequently filtered out for polymerase chain reaction (PCR) duplicates by Samtools (version 0.1.18)[24] locally realigned around inferred insertions and deletions, and their base qualities recalibrated in the context of alignment by Genome Analysis Toolkit (version 1.4-21).[25]

Single-nucleotide polymorphisms, short insertions, and deletions were identified by the GATK Unified Genotyper. Resulting variants were filtered out for possible sequencing and alignment artifacts, taking into consideration variant quality, variant read-depth, and the proportion of not-uniquely-mapped reads overlapping variants (supplemental Table 1). Prediction tracks for each mutation were generated by automatic queries to Mutation Taster[26] and PolyPhen-2.[27] Output data were filtered on the basis of an autosomal dominant model of inheritance, removing those annotated variants which were out-of-exome target, synonymous, common (as annotated in dbSNP135), or found in previous exome sequencing of uncorrelated samples. Candidate variants were also compared and prioritized with the 1000 Genome Project Database and the Exome Sequencing Project (ESP) Database (Exome Variant Server, HLBI ESP, Seattle, WA; ESP5400 release). The remaining, filtered variants were assessed for pathogenicity by SIFT.[28] The filtered exome sequencing data were graphically visualized with Integrative Genomics Viewer, allowing interactive exploration of these genomic datasets.[29]

RNA isolation and cDNA synthesis from CD34$^+$ cells

Total RNA was isolated[30] from CD34$^+$ cells at days 0, 7, and 14 of erythroid differentiation. Single-strand complementary DNA (cDNA) was synthesized from 2 μg of RNA template, using 2.5 units of VILO reverse transcriptase (Life Technologies, Milan, Italy).

Two microelectrode voltage clamp of PIEZO1-expressing oocytes

Oocytes were harvested from *Xenopus laevis* and treated with collagenase as previously described.[31-34] cRNA was injected in a volume of 50 nL, and oocytes were maintained at 17°C for 72 hours prior to experimentation. Defolliculated oocytes were placed in ND96 (in mM, 96 NaCl, 2 KCl, 1.8 $CaCl_2$, 1 $MgCl_2$, 5 HEPES [*N*-2-hydroxyethylpiperazine-*N*′-2-ethanesulfonic acid], pH 7.4) in a bath (RC-16; Warner Instruments, Hamden, CT) on the headstage of an upright microscope and imaged at ×20 magnification. Oocytes were impaled with pipettes fabricated from borosilicate glass (World Precision Instruments, Sarasota, FL) using a Sutter P87 puller. Resistances of electrodes were 2 to 10 megaohms when filled with 3M KCl.

A voltage clamp protocol was generated using the Clampex subroutine of PCLAMP 10 (Molecular Devices Corporation, Sunnyvale, CA), applying 10 sweeps of 400 ms, in 20-mV steps from −70 mV, with a sampling rate of 10 kHz. Holding potential was −30 mV in all groups throughout the experiment. Currents were recorded using a Geneclamp 500 voltage clamp (Molecular Devices). The bath reference electrode was a silver chlorided wire with a 3M KCl agar bridge. Junction potentials were minimized by using 3M KCl in the pipettes and by use of a bath clamp.

Table 1. *PIEZO1* mutations found in the families here analyzed

Family (code)	DHSt	FP	PO	Nucleotide mutations	Amino acid mutations*	Genotype		Reference
						Allele 1*	Allele 2	
Arras (AR)	+	+		c.7463 G>A	**p.R2488Q**	**p.R2488Q**	WT	15
				c.2152 G>A	**p.G718S**	**p.G718S**	WT	
Edinburgh	+	+		c.6380 C>T	**p.T2127M**	**p.T2127M**	WT	20
Essex	+			c.3350 C>T	**p.S1117L**	**p.S1117L**	WT	14
				c.6059 C>T	**p.A2020V**	**p.A2020V**	WT	
Dax (DA)	+			c.6495-6508delAGA	**p.2166-2169 delK**	**p.2166-2169 delK**	WT	15
Bicetre (BI)	+	+	+	c.1848+31C>G			WT	15
				c. 2344 G>A	**p.G782S**	**p.G782S**	WT	
				c. 2423 G>A	**p.R808Q**	**p.R808Q**	WT	
Troyes (TR)	+			c.6008 C>A	**p.A2003D**	**p.A2003D**	WT	15
San Francisco (SF)				c.7367 G>A	p.R2456H	p.R2456H	WT	Unpublished

PO, perinatal edema; +, presence of the clinical characteristics.
*Novel mutations are highlighted in bold.

Current voltage relationships were determined by fitting the currents recorded at t = 370 ms using the Clampfit subroutine of PCLAMP 10, and plotted with Sigmaplot graphics.

On-cell patch recording of PIEZO1-expressing oocytes

Defolliculated oocytes were placed in a hypertonic bath and the vitelline layer was removed by hand with Dumont no. 5 forceps under ×40 magnification. The devitellinized oocyte was immediately placed in a low-volume bath (RC-25; Warner Instruments) on the stage of an Olympus IMT-2 inverted microscope, imaged at ×40 and patched with fire-polished pipettes of 7 to 12 megaohms resistance. Bath and pipette solutions contained (in mM) 150 Na methanesulfonate, 10 Na EDTA, and 10 Na HEPES, pH 7.4. On-cell patch recording was performed as previously described in this paragraph, except that currents were elicited by imposition of a 250-ms linear voltage ramp from −100 mV to +100 mV during application of negative pressure (0 or −25 mm Hg) to the pipette port and recorded by pneumatic transducer (Biotek DPM-1B, Winooski, VT).

Results

Whole-exome analysis

Whole-exome analysis was performed on 2 affected and 2 unaffected members from family Edinburgh (DHSt plus pseudohyperkalemia). After filtering out of likely false-positive single-nucleotide variations (SNVs) and short insertions/deletions (InDels), an average of 32 362 variants was called for each of the 4 exomes, spanning about 12 053 genes, with about 1700 novel SNVs/InDels per sample. Among novel SNVs/InDels, we focused on heterozygous variants falling in exons, splice-site junctions and 5′ and 3′ untranslated regions that segregated with disease among the 4 individuals and were absent from 38 unrelated exomes from our internal database. This approach highlighted 13 variants in as many genes, 7 of which were exonic, 5 of which were predicted as likely pathological by the in silico tools Mutation Taster, PolyPhen-2, and SIFT (supplemental Table1). One of these variants mapped within the previously defined critical region on chromosome 16,[20] and was identified as c.6380C>T, T2127M of *PIEZO1* (Table 1).

PIEZO1 mutational analysis

We sequenced *PIEZO1* in 26 affected and 16 healthy subjects among 7 affected families. The pedigrees from previous studies[14,15,20] are illustrated in supplemental Figure 2. The mutations and the number of affected and unaffected subjects are described in Table 1. The nucleotide changes are shown in Figure 1A. None of the noted nucleotide changes were present in the 1000 genomes database, or in 50 healthy subjects here analyzed. The amino acids affected by the *PIEZO1* missense mutations identified in the DHSt patients are located in 2 regions of the 2521 amino acid PIEZO1 polypeptide: 1 between residues 718 and 1117, and the carboxy-terminal region beyond residue 2000 (Figure 1B). The DHSt phenotype in families AR, Essex, and BI cosegregated with >1 novel missense mutation in *cis* in *PIEZO1* (Table 1). The mutated amino acid residues are all conserved in PIEZO1 of macaque and mouse; 9 of the 10 residues are conserved in rat PIEZO1, and 7 of the 10 are conserved in *Xenopus tropicalis* and *Danio rerio* (Figure 1C).

PIEZO1 expression in human and mouse during fetal and embryonic development

We analyzed PIEZO1 expression in several mouse and human tissues during embryonic development to account for the erythroid involvement of DHSt and for the fluid effusions occurring in some DHSt families. We collected mouse embryos at embryonic day (E) 9.5, E10.5, E12.5, E15.5 and postnatal day 0 (P0; at birth) for quantitative PCR analysis of murine *PIEZO1* expression. PIEZO1 messenger RNA (mRNA) abundance increased gradually from E9.5 to E15.5 and was sustained through birth (Figure 2A-B).

We further showed PIEZO1 polypeptide expression in adult RBC membranes from mice (Figure 2C) and humans (Figure 2D).

PIEZO1 immunohistochemical analyses were performed on human fetal tissues (17 weeks of gestation) to verify PIEZO1 expression in liver, spleen, and peritoneum lymphatic vessels. In fetal liver, PIEZO1 showed strong cytoplasmic and membrane signals particularly in hepatic erythroblasts. Fetal spleen at 17 weeks showed positive cytoplasmic staining patterns in splenic plasma cells. We also analyzed PIEZO1 expression in lymphatic vessel of fetal peritoneum at gestational week 17 to examine the correlation between PIEZO1 expression and occurrence of perinatal edema. PIEZO1 showed a marked signal in lymphatic vessels (Figure 2E). In contrast, PIEZO1 immunoreactivity was absent from peritoneal lymphatic vessels of healthy human adult subjects. This observation provides a first link between *PIEZO1* mutations and pre- or perinatal edema.

PIEZO1 expression and localization in RBCs

PIEZO1 localization in RBCs was evaluated in healthy controls. Confocal microscopy analysis showed that PIEZO1 was expressed on the RBC membrane, as demonstrated by its complete colocalization with the erythroid membrane marker glycophorin A (Figure 3A), and

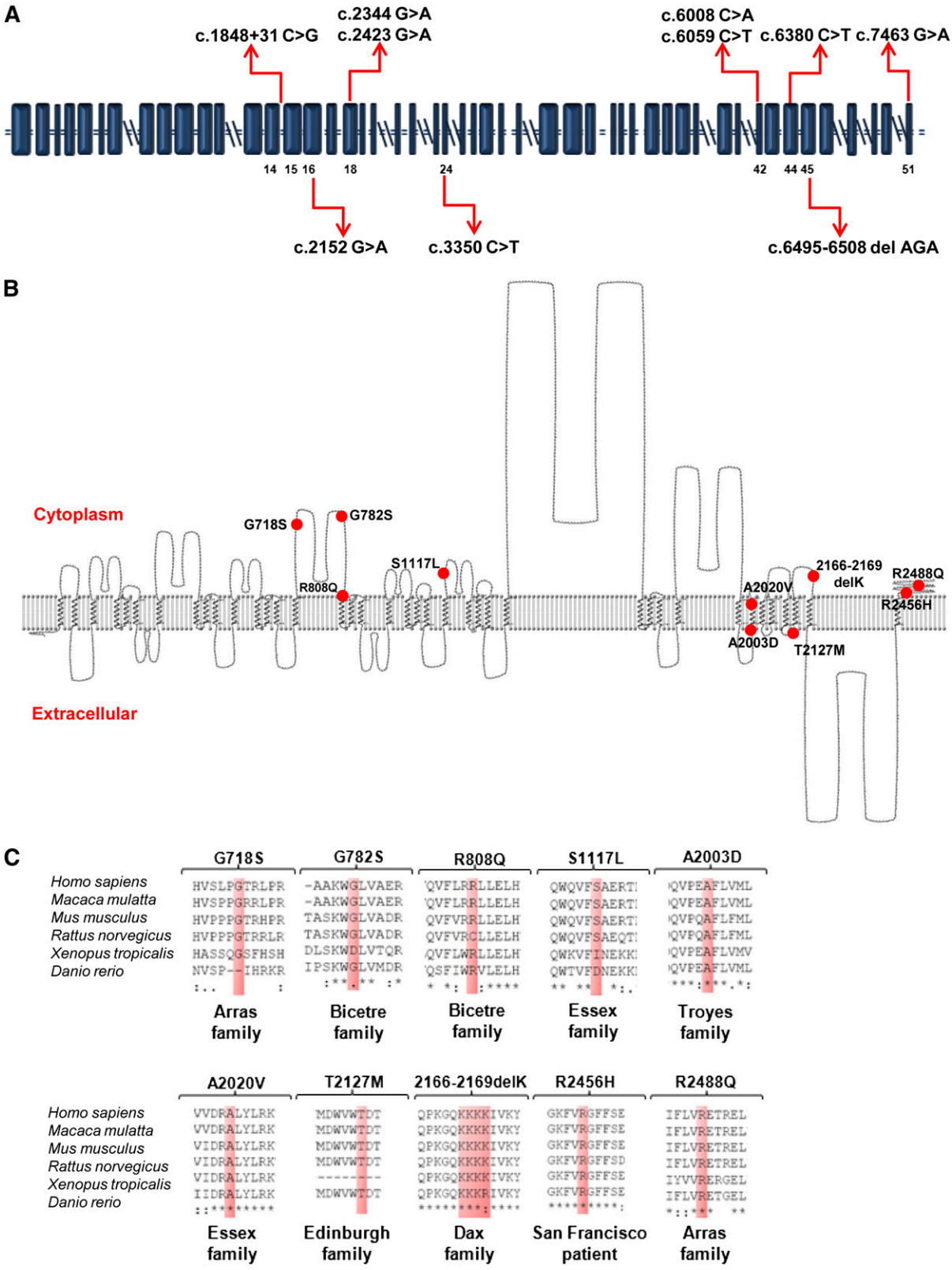

Figure 1. Mutational analysis. (A) Schematic representation of *PIEZO1* (blue squares, exons; horizontal double lines, introns; double slashes, large introns); red arrows indicate exonic positions of the nucleotides mutated in the 7 families in whom DHSt was previously mapped to chromosome 16q. (B) A 2-dimensional (2D) hydropathy profile of human PIEZO1 protein. The transmembrane regions of PIEZO1 (UniProt accession Q92508) predicted by TMHMM were displayed using TMRPres2D. Red circles mark approximate locations of DHSt-associated missense mutations. (C) Evolutionary conservation of the residues mutated in our DHSt patients (red-shaded boxes) among the species indicated at left.

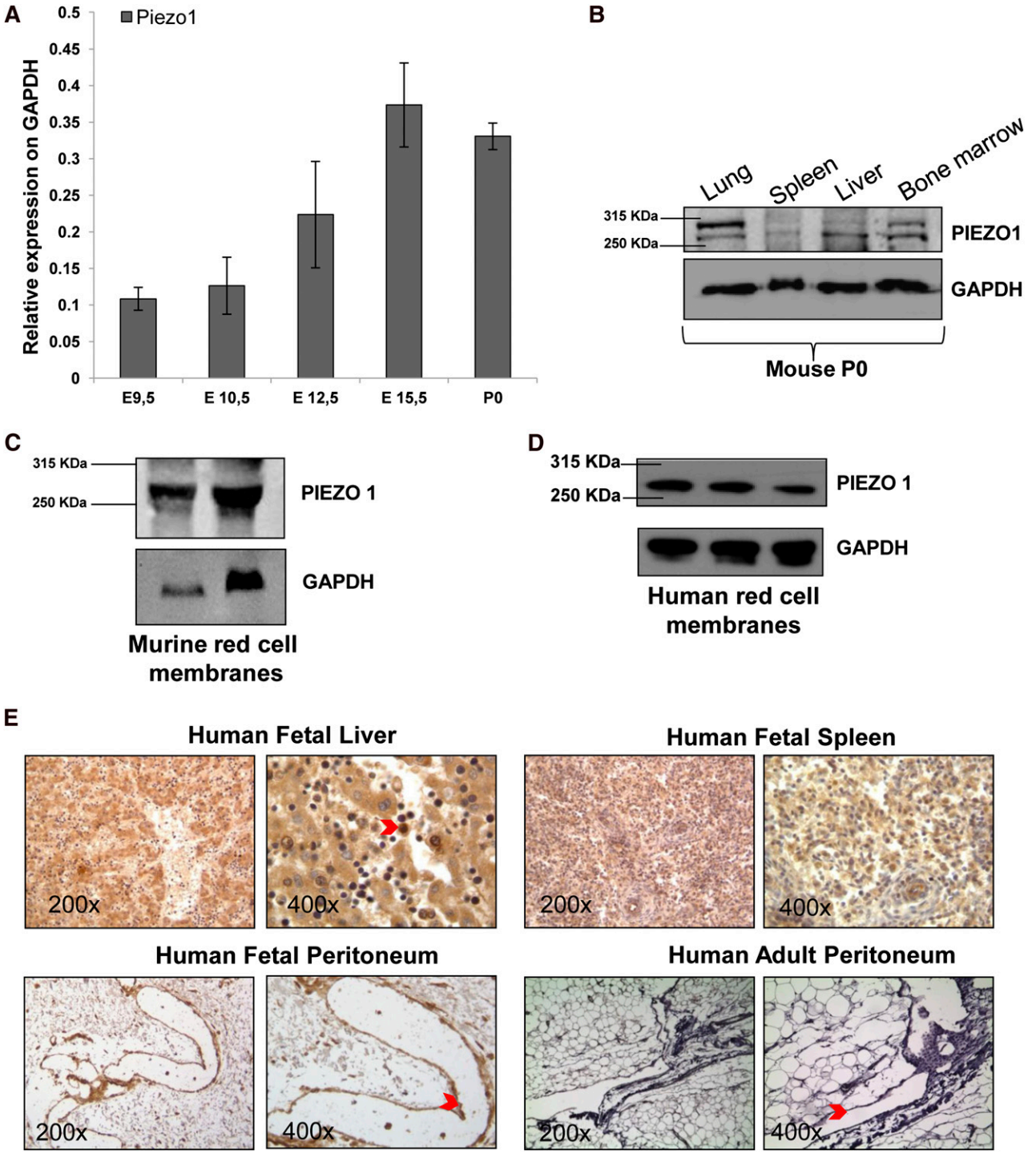

Figure 2. PIEZO1 characterization during mouse and human embryonic development. (A) PIEZO1 mRNA levels (normalized to GAPDH) in murine C57BL/6 embryos at E9.5, E10.5, E12.5, E15.5 and P0. Mean + SEM of 3 experiments. (B) Immunoblot showing expression of PIEZO1 protein expression in lung, spleen, liver, and bone marrow from P0 C57BL/6 mouse. Protein (50 μg) was loaded in each lane, with GAPDH as loading control. Representative of 2 independent fresh tissue lysate preparations. (C) Immunoblot showing PIEZO1 protein RBC membranes prepared from blood pooled from 8 adult C57BL/6 mice. Protein (50 or 100 μg) was loaded in each lane, with GAPDH as loading control. One of 3 similar experiments with independent membrane preparations. (D) Immunoblot showing PIEZO1 protein in human RBC membranes prepared from blood pooled from 3 healthy subjects for each lane. Protein (50 μg) was loaded in each lane, with GAPDH as loading control. One of 3 similar experiments with independent membrane preparations. (E) Immunohistochemical expression in human fetal (17 weeks of gestations) and adult tissues with PIEZO1 rabbit polyclonal antibody. The red arrow in the ×400 liver panel indicates a positive erythroblast. The red arrows in the fetal peritoneum panels indicate positive staining in the lymphatic vessels, while in the adult peritoneum panels indicate negative staining in the lymphatic vessels. Antigen is stained brown; nuclei are stained in purple with hematoxylin. Tissues were imaged with a Leica microscope equipped with 20× and 63× objectives. Representative of 3 independent experiments. GAPDH, glyceraldehyde-3-phosphate dehydrogenase.

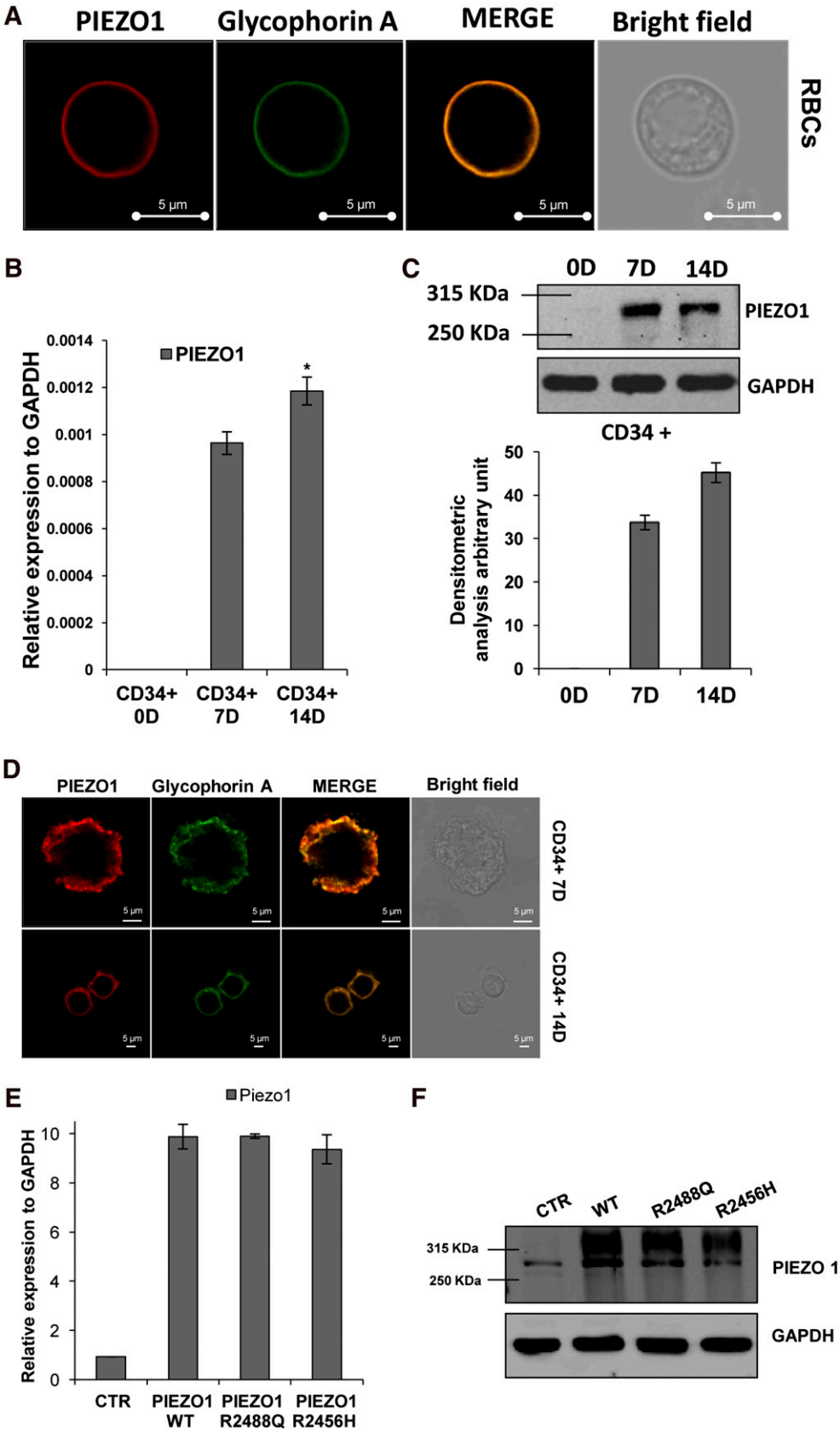

Figure 3. PIEZO1 characterization in RBCs and in CD34$^+$ blood cells during erythroid differentiation. (A) Laser-scanning confocal immunofluorescence images of a peripheral blood smear from a control subject stained with rabbit polyclonal antibody to PIEZO1 (red) and mouse monoclonal antibody to glycophorin A (membrane marker, green), showing colocalization of the 2 signals (merge), and a bright-field image of a red cell. Cells were imaged with a Leica TCS SMD FLIM confocal microscope equipped with a 1.4 NA oil-immersion HCX PL APO CS 100× objective. Luminosity and contrast were uniformly adjusted with Axiovision software. Representative of 3 independent experiments. (B) PIEZO1 mRNA levels (normalized to GADPH) in CD34$^+$ cells induced to erythroid differentiation by EPO at 0, 7, and 14 days by quantitative reverse transcription PCR. **P* value, .003 (CD34$^+$ 14D vs CD34$^+$ 7D). (C) Immunoblot of PIEZO1 protein in lysate of CD34$^+$ cells induced to erythroid differentiation at 0, 7, and 14 days (50 μg of protein; GAPDH was loading control). The graph below shows densitomteric analysis of this and similar blots. (D) Laser-scanning confocal microscopy images of CD34$^+$ cells induced to differentiation at 7 and 14 days by EPO, showing colocalization of PIEZO1 (red) and glycophorin A (green). Cells were imaged with a Leica TCS SMD FLIM confocal microscope equipped with a 1.4 NA oil-immersion HCX PL APO CS 63× objective. Bright-field images show the morphology of CD34$^+$ cells after 7 or 14 days of erythroid differentiation. Luminosity and contrast were adjusted using Axiovision software. (E) PIEZO1 mRNA levels (normalized to GAPDH) in HEK-293 cells transiently transfected (72 hours) with empty vector or with cDNA encoding WT PIEZO1 or PIEZO1 mutants R2488Q and R2456H. Mean + SEM of 3 experiments. (F) Immunoblot of PIEZO1 polypeptide in HEK-293 cells transiently transfected (72 hours) with empty vector or with cDNA encoding WT PIEZO1 or PIEZO1 mutants R2488Q and R2456H. GAPDH serves as loading control. One of 2 similar experiments.

confirmed by colocalization with the membrane marker CD55/DAF (supplemental Figure 3; negative control immunofluorescence experiments are shown in supplemental Figure 4).

The data confirm previous mass spectrometry data of Zarychanski et al[18] showing the presence of PIEZO1 protein in red cell membranes.

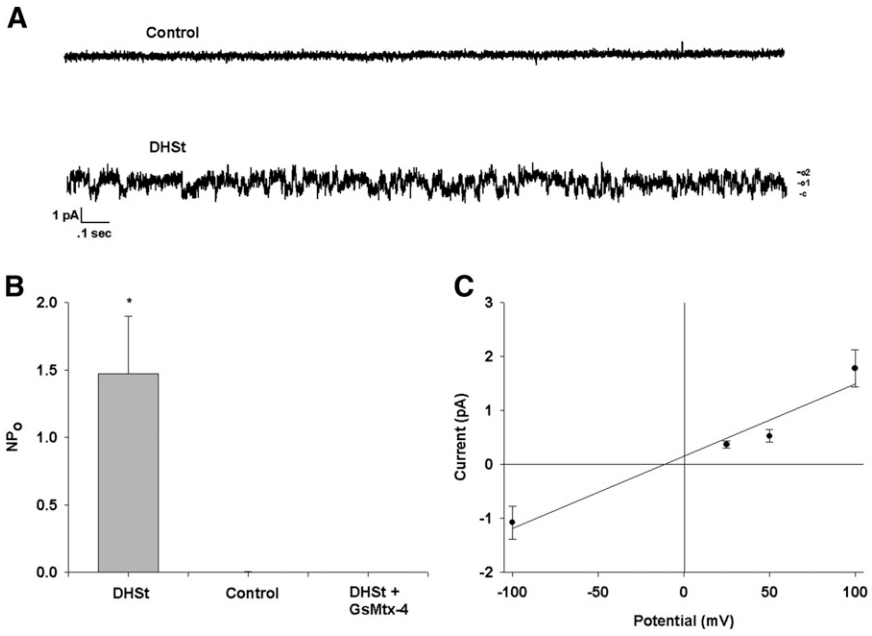

Figure 4. Cation channel activity in on-cell patch recordings of DHSt red cells from patient SF. (A) Representative graphs of channel activity in on-cell patches from an unrelated normal cell (above) and a DHSt red cell from patient SF. (B) NPo of channel activity in DHSt red cells from patient SF (n = 4), from an unrelated volunteer (Control, n = 3) and from patient SF in the presence of pipet GsMTx-4 (2.5 μM; n = 3); $*P < .05$. (C) I-V curve of a representative on-cell patch record from a DHSt red cell of patient SF.

PIEZO1 expression during erythroid differentiation

To investigate the role of PIEZO1 in erythroid cells, we first examined PIEZO1 expression and localization in an ex vivo model of erythroid differentiation. $CD34^+$ cells isolated from the peripheral blood of healthy volunteers were induced to erythroid differentiation by 14 days of erythropoietin treatment, as detailed in "Materials and methods." As shown in Figure 3B, PIEZO1 mRNA was significantly upregulated after 14 days of erythropoietin treatment ($P = .003$). These data were confirmed at the protein level by western blotting and densitometric analysis (Figure 3C).

We then assessed PIEZO1 protein localization in the same cell systems. As shown in Figure 3D, PIEZO1 colocalized with the plasma membrane marker glycophorin A at 7 and 14 days of $CD34^+$ erythroid differentiation (Figure 3D). No PIEZO1 immunoreactivity was detected in day 0 $CD34^+$ cells (not shown).

Expression of WT and mutant PIEZO1 polypeptides in HEK-293 cells

To evaluate expression of the PIEZO1 mutants, we cloned PIEZO1 wild-type (WT) and PIEZO1 mutants R2488Q and R2456H in pCMV6-IRES-GFP and transiently transfected the recombinant plasmids into HEK-293 cells. We found that neither mutation impaired PIEZO1 expression at mRNA or protein levels (Figure 3E-F).

DHSt red cells exhibit altered ion content and transport

Patient SF red cells heterozygous for the PIEZO1 mutation R2456H had elevated Na content of 61 mmol/kg Hb and reduced K content of 219 mmol/kg Hb (after overnight shipment). Magnesium (Mg) content was slightly elevated at 9.7 mmol/kg Hb. Red cell activities of K-Cl cotransport, Na-K-2Cl cotransport, and Na/H exchange were not higher than in unrelated control cells (not shown). On-cell patches recorded from patient SF DHSt red cells as described in "Materials and methods" (Figure 4A) revealed spontaneous ion-channel activity (lower trace) not detected in cells from an unrelated subject (upper trace). This activity was characterized by a distribution of channel open probability (NPo) of 1.47 + 0.43 (Figure 4B), a single-channel ohmic conductance of 13 single channel conductance (pS) with reversal potential −11 mV ($r^2 = 0.95$; Figure 4C), and was competely blocked by 2.5 μM *Grammastola spatulata* mechanotoxin-4 (GsMTx4) in the pipet ($P < .05$).

Function of WT and mutant *PIEZO1* expressed in *Xenopus* oocytes

X laevis oocytes previously injected with hPIEZO1 complementary RNA (cRNA) were subjected after 72 hours to 2-electrode voltage clamp recording. Uninjected oocytes exhibited a small linear current at holding potentials between −100 and +80 mV, with reversal potential of −64 mV (Figure 5A). After 14 minutes of exposure to a moderately hypotonic bath (20% dilution of ND-96 which, based on the low intrinsic oocyte water permeability[35] should produce only minimal swelling), these properties remained essentially unchanged. Oocytes previously injected with PIEZO1 cRNA exhibited slightly elevated currents in ND-96, but with a reversal potential depolarized to −40 mV. However, and in contrast to uninjected oocytes, 14-minute exposure of PIEZO1-expressing oocytes to hypotonic bath conditions substantially increased an outwardly rectifying current, while hyperpolarizing reversal potential to −56 mV (Figure 5A). Exposure of oocytes previously injected with PIEZO1 cRNA to hypertonic bath (ND-96 containing 200 mM mannitol, 15 minutes) also led to increased current (not shown).

Because mPIEZO1 exhibits mechanosensitivity, multichannel on-cell patch currents of *Xenopus* oocytes expressing hPIEZO1 were recorded during voltage ramps before and during application of −25 mm Hg suction via pipet. As shown in Figure 5B, negative pressure did not alter current in uninjected oocytes. In contrast, negative pressure induced increased currents in oocytes expressing PIEZO1 ($P < .005$) and mutant R2488Q ($P < .001$), but not mutant R2456H (Figure 5C). The response of mutant R2488Q to negative pressure appeared to exceed that of WT PIEZO1 ($P = .057$).

Occasional oocyte patches allowed resolution of single-channel activity, as illustrated in Figure 6 and in supplemental Figure 5. In these resting state patches, the uninjected oocyte NPo of 0.013 increased to 0.69 in oocytes expressing WT PIEZO1, 0.88 in oocytes expressing PIEZO1 mutant R22488, and 0.22 in oocytes expressing mutant R2456H. Respective single-channel conductances were 25 pS (WT), 26.5 pS (R2488Q), and 43 pS (R24566H).

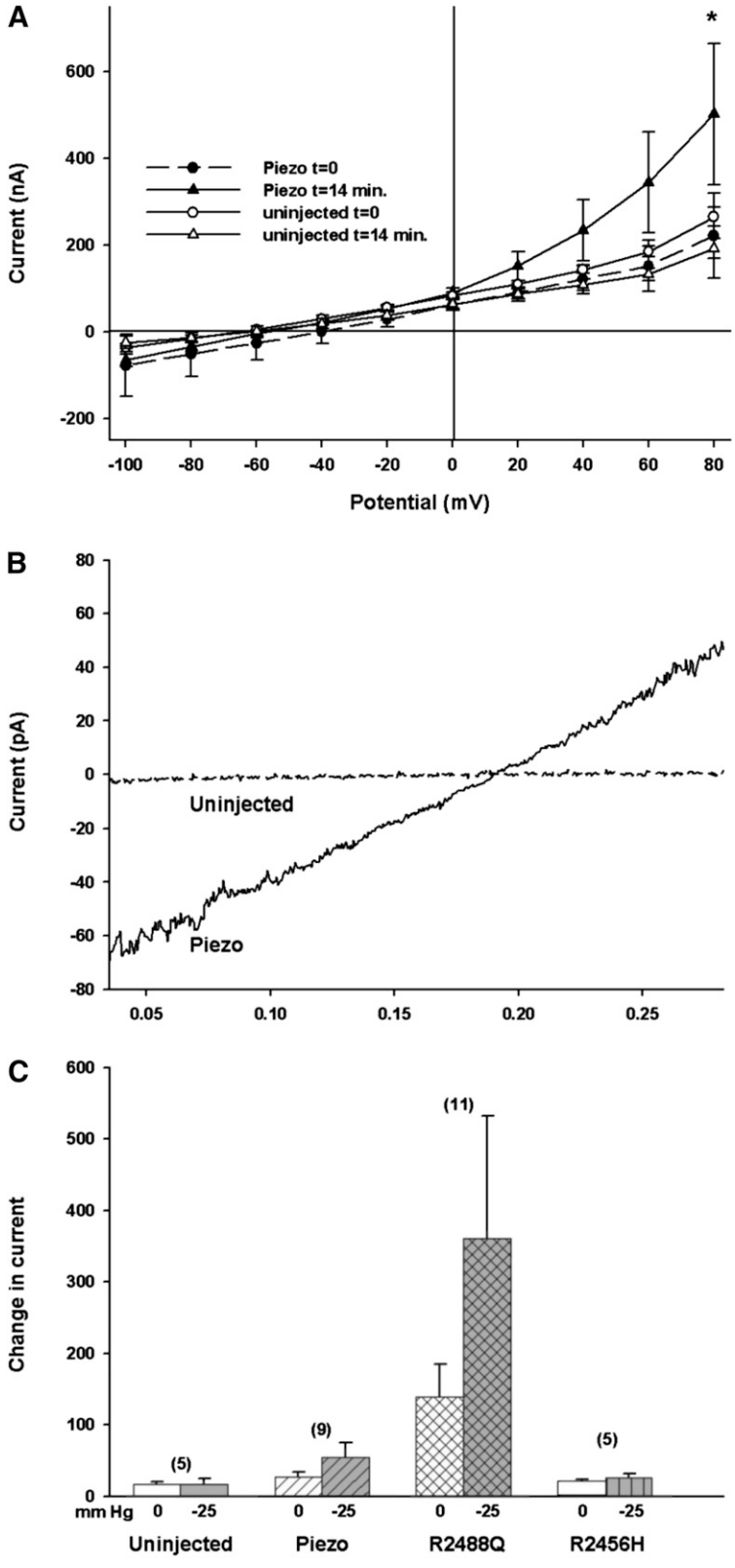

Figure 5. PIEZO1 expressed in *Xenopus* oocytes confers increased current elicited by hypotonic medium and negative pressure activates currents in on-cell membrane patches of WT PIEZO1 and mutant R2488Q. (A) Current-voltage relationship of 2-electrode voltage clamp records from uninjected oocytes or oocytes previously injected with cRNA encoding PIEZO1, before and 14 minutes after bath change to a slightly hypotonic solution (ND-96 diluted 20% with distilled water). (B) On-cell patches were established on surface membranes of uninjected *Xenopus* oocytes or oocytes previously injected with cRNA encoding WT PIEZO1 or mutants R2488Q or R2456H. Currents were recorded during 250-msec voltage ramps between −100 mV and +100 mV. Representative traces from an uninjected oocyte and an oocyte expressing WT PIEZO1 during pipet application of −25 mm Hg hydrostatic pressure. (C) Bar graph of the magnitidue of the current differences between values recorded at −100 and +100 mV in on-cell patches from (n) uninjected oocytes or oocytes previously injected with cRNAs encoding WT PIEZO1 or the indicated mutants, in voltage ramp experiments such as shown in panel A. At −25 mm hydrostatic pressure, uninjected oocytes differed from oocytes expressing WT PIEZO1 or mutant R2488Q, but not from mutant R2456H ($P < .05$, Kruskal-Wallis ANOVA with the Dunn post-test).

Discussion

We have identified *PIEZO1* as the causative gene for the varied clinical forms of autosomal dominant DHSt linked to chromosome 16p. *PIEZO1* was selected as a strong candidate gene within the critical region previously mapped to 16q23-qter based on exome sequencing analysis in family Edinburgh. Subsequent targeted sequencing analysis identified several additional novel *PIEZO1* mutations in 7 families with DHSt syndromes. PIEZO1 protein

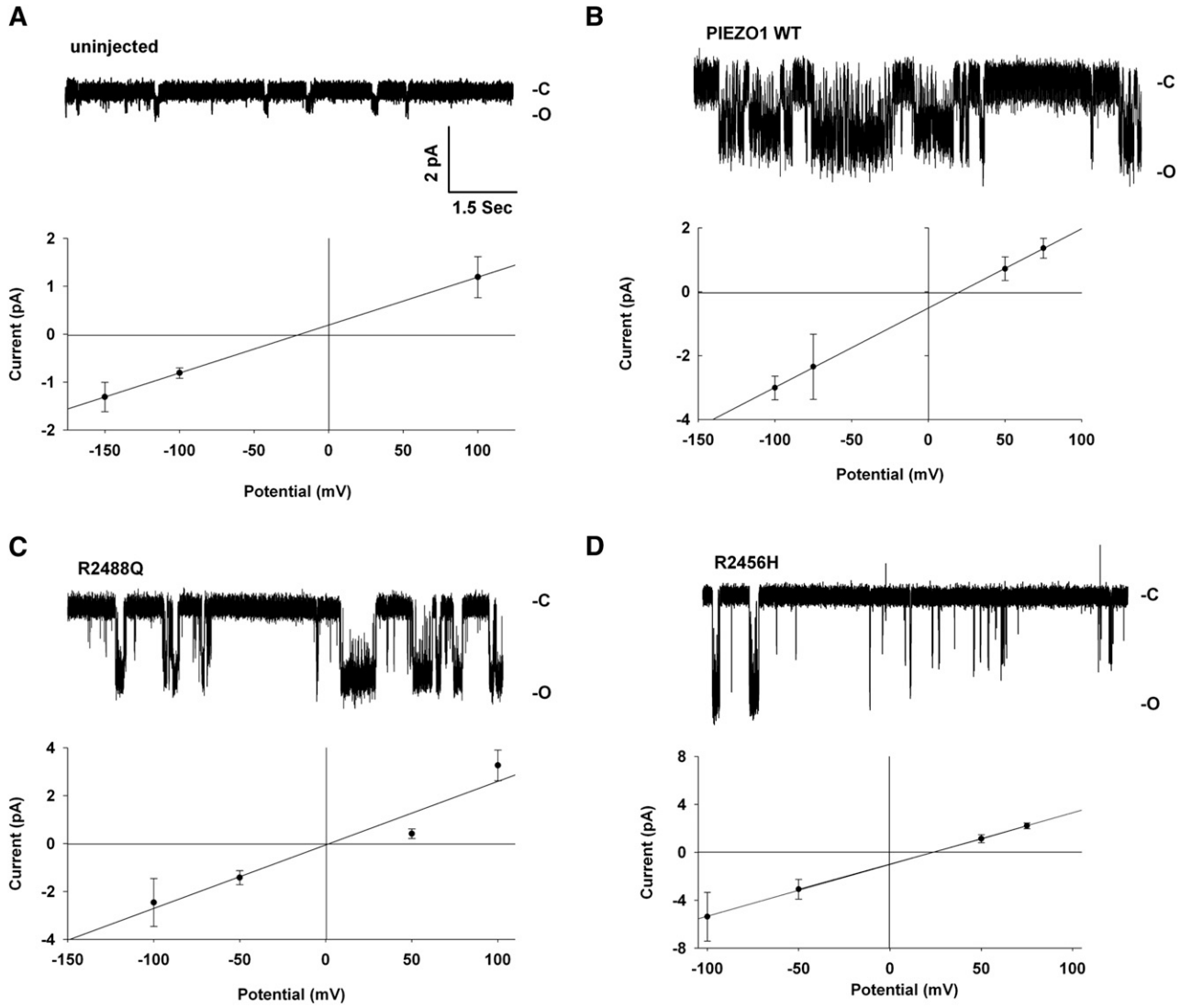

Figure 6. On-cell patch current traces of R2488Q and R2456H mutations in *Xenopus* oocytes. On-cell patch current traces (recorded at −applied voltage at the membrane patch (VP) = −100 mV) and current-voltage relationships from (A) uninjected oocytes and (B) oocytes previously injected with cRNA encoding WT PIEZO1, (C) PIEZO1 mutant R2488Q, and (D) PIEZO1 mutant R2456H. Single-channel slope conductances are 25 pS (wildtype), 26.5 pS (R2488Q), and 43 pS (R2456H). Supplemental Figure 3S presents a higher resolution on-cell patch trace from an oocyte expressing mutant R2456H.

expression was characterized during human and murine development and during erythroid differentiation. Functional studies demonstrated for the first time that *PIEZO1* mutations cause altered ion transport in erythroid cells. PIEZO1 protein was also detected in fetal lymphatic vessel endothelium, consistent with its proposed causative role in the pathogenesis of perinatal effusions. Electrophysiology analysis in oocytes demonstrated changes in ion transport consistent with the altered ion content of DHSt patient red cells. A flowchart illustrating our study design is shown in supplemental Figure 6.

The *PIEZO1* open reading frame was first found in the human immature myeloid cell line KG-1, and transcript tissue profiles showed apparently ubiquitous expression.[36] Satoh et al demonstrated transcriptional induction of PIEZO1 in senile plaque-associated astrocytes from Alzheimer disease patients.[37] PIEZO1 involvement in integrin activation requires recruitment to the endoplasmic reticulum of the small GTPase *R*-Ras, promoting release of Ca^{2+} from intracellular stores to activate cytoplasmic calpain.[38] Recently, PIEZO1 and PIEZO2 were both implicated in mechanosensation as stretch-activated cation channels.[39-42] Soon thereafter, expression in human cells of the single *Drosophila melanogaster* PIEZO (DmPIEZO or CG8486) was shown to resemble its mammalian counterparts in its ability to induce mechanically activated currents.[43] Behavioral responses to noxious mechanical stimuli were severely reduced in DmPIEZO knockout larvae, whereas responses to light touch or to other types of noxious stimulus were unaffected. Human PIEZO1 is an N-linked glycoprotein[44] that serves as substrate for both acetylation[45] and phosphorylation.[46,47] Coste et al further showed that mouse PIEZO (MmPIEZO1) can assemble as a 1.2-megadalton homo-oligomer with a total of 120 to 160 transmembrane segments, the largest homomeric plasma membrane ion-channel complex identified to date.[39] Purified MmPIEZO1 reconstituted into asymmetric lipid bilayers and liposomes forms ruthenium-red–sensitive ion channels in the absence of any other protein.[39]

We here characterized PIEZO1 expression during mouse and human development. We have shown that PIEZO1 expression increased during murine embryogenesis and, at birth, expression was predominant in liver and bone marrow. In fetal human tissues, PIEZO1 showed marked expression in liver and spleen. Of note, PIEZO1 was expressed in lymphatic vessels of the fetal peritoneum and was absent in adult lymphatic vessels, demonstrating for the first time a potential physiological link between PIEZO1 mutations and the perinatal edema that sometimes accompanies DHSt.

We also identified PIEZO1 expression and localization in the plasma membrane of RBCs, confirming immunologically the original mass spectroscopic identification of PIEZO1 as part of the red cell membrane proteome,[48] and its subsequent detection in red cell membrane by targeted mass spectrometry.[18]

In 3 unrelated families, we found multiple in *cis* missense mutations in *PIEZO1*. R2488Q mutation in family Arras altered a residue conserved in all analyzed species (Figure 1C), and the linked mutation G718S altered a residue conserved in all tested species except *D rerio*. A2020V mutation in family Essex altered a completely conserved residue, and linked mutation S1117L altered a residue conserved in all tested species except *X tropicalis* and *D rerio*. The linked variants at sites of lesser evolutionary conservation are not, however, present among normal alleles and SNV databases, and so may not be harmless variants. Further studies will elucidate the origin of geographic clustering of these mutations. However, the contribution of each individual mutation to its linked clinical phenotype cannot yet be assigned. At this time, we do not know which one of the mutations coinherited in *cis* might be individually responsible for the disease phenotype, or whether disease arises from the combined effects of the coinherited mutations. Interestingly, the 2 families carrying 2 novel, linked mutations exhibited the phenotype of DHSt plus pseudohyperkalemia, but affected individuals in the single family characterized by 3 allelic mutations exhibited a more complex phenotype of DHSt plus perinatal edema and pseudohyperkalemia. The connections linking genotype to the red cell dehydration phenotype and to phenotypic variability could reflect mutation position within the 3-dimensional structure of the PIEZO1 polypeptide (allelic heterogeneity) and/or modifier gene coinheritance.

Patient SF exhibited the same mutation, R2456H, found in one of the families reported by Zarychanski et al.[18] Our patient and the previously reported R2456H patients showed a similar phenotype characterized by DHSt unaccompanied by pseudohyperkalemia or perinatal edema. In contrast to the report of Zarychanski and colleagues, our families exhibited only heterozygous mutations, as predicted for a simple pattern of dominant inheritance.

The presence of PIEZO1 in the red cell membrane suggests a link to the erythroid ion imbalance and altered erythroid ion-channel activity of DHSt patients. Functional studies in *Xenopus* oocytes demonstrated that WT PIEZO1 expression increased 2-electrode voltage clamp current elicited by osmotic swelling, and channel activity in cell-attached patches. The PIEZO1 mutation R2488Q increased hydrostatic pressure-induced currents in on-cell patches of *Xenopus* oocytes, likely reflecting, in part, increased NPo. Oocytes expressing PIEZO1 mutant R2456H exhibited cell-attached patch currents of elevated single-channel conductance. These properties of oocytes expressing PIEZO1 mutants are consistent with the steady-state elevation of intracellular Na^+ and reduction of intracellular K^+ that characterize red cells of DHSt patients. However, the link between PIEZO1 mutations and the combination of elevated MCV and mean corpuscolar Hb concentration which underlie the descriptor "dehydrated stomatocytosis" will require further experimentation. Further experiments will be needed to confirm individual mutation-selective changes in single-channel characteristics suggested by the present data. Detailed comparison of functional effects of endogenous WT and mutant PIEZO1 in intact red cells with those of heterologous WT and mutant PIEZO1 expressed in *Xenopus* oocytes will also require additional experiments. These will be directed toward a greater understanding of differences between the chronic effects and influences of WT and mutant PIEZO1 channels on cell volume and ion content and the rapid kinetics of PIEZO1 channels recorded in whole-cell and patch modes. Such differences are influenced by the still incompletely defined changes in membrane tension and cytoskeletal dynamices inside the patch pipet containing the distinct plasma membranes of fetal erythrocytes, adult erythrocytes, and *Xenopus* oocytes. All of these, in turn, likely differ from the strains experienced by the membranes of intact red cells over their normal 120-day lifespan as they experience a range of laminar and turbulent shear stresses during their circulation through vessels ranging in diameter from the ventricular chamber and the aorta to capillary tortuosities, and accompanied by sequential adhesions to and releases from other blood cells and endothelial cells.

In conclusion, DHSt is a pleiotropic syndrome caused by dominant *PIEZO1* mutations. In particular, R2456H and R2488Q mutations in *PIEZO1* likely alter mechanosensitive channel regulation, leading to increased cation transport in erythroid cells. Ongoing functional analysis should further elucidate the pathogenic mechanisms of all *PIEZO1* mutations found in simple and syndromic forms of DHSt.

Acknowledgments

The authors thank the CEINGE Service Facility platforms including the Dynamic Imaging Facility (particularly Dr Daniela Sarnataro for providing helpful technical support), the Sequencing Core, the Comparative Pathology Facility, and the FACS Core Laboratory. In addition, the authors thank Prof M. d'Armiento (Federico II University of Naples) for expert immunohistochemical and cell compartment analysis, and Dr Eduardo Nusco (Tigem, animal housing) for the kind gift of C57BL/6 embryos.

This work was supported by Italian Ministero dell'Università e della Ricerca (MIUR), by Telethon (Italy) (GGP09044; A.I.), by Regione Campania contract grant no. DGRC 1901/200 (A.I.), and by the Doris Duke Charitable Foundation (S.L.A.).

This study was approved by the Institutional Review Board Telethon (Italy) and conducted in accordance with the Declaration of Helsinki.

Authorship

Contribution: I.A., S.L.A., L. De Franceschi, J.D., and A.I. designed and conducted the study, and prepared the manuscript; C.B. contributed to the preparation of the manuscript; C.A., R.R., L. De Falco, M.R.E., B.E.S., D.H.V., and F.V. performed sequencing analysis and functional studies; D.M. performed

immunohistochemical analysis; M.D. performed immunohistopathology analyses; A.V., I.L., and O.Z. performed the exome sequencing analysis; R.N., S.L.S., and B.E.G. performed clinical evaluation of patient SF; and G.W.S. provided Edinburgh family samples and contributed to critical review of the manuscript.

Conflict-of-interest disclosure: The authors declare no competing financial interests.

Correspondence: Achille Iolascon, CEINGE, Biotecnologie Avanzate, Via Gaetano Salvatore, 486 80145 Naples, Italy; e-mail: achille.iolascon@unina.it.

References

1. Oski FA, Naiman JL, Blum SF, et al. Congenital hemolytic anemia with high-sodium, low-potassium red cells. Studies of three generations of a family with a new variant. *N Engl J Med.* 1969; 280(17):909-916.
2. Miller DR, Rickles FR, Lichtman MA, La Celle PL, Bates J, Weed RI. A new variant of hereditary hemolytic anemia with stomatocytosis and erythrocyte cation abnormality. *Blood.* 1971;38(2): 184-204.
3. Stewart GW. Hemolytic disease due to membrane ion channel disorders. *Curr Opin Hematol.* 2004; 11(4):244-250.
4. Delaunay J. The hereditary stomatocytoses: genetic disorders of the red cell membrane permeability to monovalent cations. *Semin Hematol.* 2004;41(2):165-172.
5. Delaunay J. The molecular basis of hereditary red cell membrane disorders. *Blood Rev.* 2007;21(1): 1-20.
6. Syfuss PY, Ciupea A, Brahimi S, et al. Mild dehydrated hereditary stomatocytosis revealed by marked hepatosiderosis. *Clin Lab Haematol.* 2006;28(4):270-274.
7. Stewart GW, Amess JAL, Eber SW, et al. Thrombo-embolic disease after splenectomy for hereditary stomatocytosis. *Br J Haematol.* 1996; 93(2):303-310.
8. Jaïs X, Till SJ, Cynober T, et al. An extreme consequence of splenectomy in dehydrated hereditary stomatocytosis: gradual thrombo-embolic pulmonary hypertension and lung-heart transplantation. *Hemoglobin.* 2003;27(3):139-147.
9. Entezami M, Becker R, Menssen HD, Marcinkowski M, Versmold HT. Xerocytosis with concomitant intrauterine ascites: first description and therapeutic approach. *Blood.* 1996;87(12): 5392-5393.
10. Grootenboer S, Schischmanoff PO, Cynober T, et al. A genetic syndrome associating dehydrated hereditary stomatocytosis, pseudohyperkalaemia and perinatal oedema. *Br J Haematol.* 1998; 103(2):383-386.
11. Grootenboer-Mignot S, Crétien A, Laurendeau I, et al. Sub-lethal hydrops as a manifestation of dehydrated hereditary stomatocytosis in two consecutive pregnancies. *Prenat Diagn.* 2003; 23(5):380-384.
12. Grootenboer S, Barro C, Cynober T, et al. Dehydrated hereditary stomatocytosis: a cause of prenatal ascites. *Prenat Diagn.* 2001;21(13): 1114-1118.
13. Andolfo I, Alper SL, Delaunay J, et al. Missense mutations in the ABCB6 transporter cause dominant familial pseudohyperkalemia. *Am J Hematol.* 2013;88(1):66-72.
14. Carella M, Stewart G, Ajetunmobi JF, et al. Genomewide search for dehydrated hereditary stomatocytosis (hereditary xerocytosis): mapping of locus to chromosome 16 (16q23-qter). *Am J Hum Genet.* 1998;63(3):810-816.
15. Grootenboer S, Schischmanoff PO, Laurendeau I, et al. Pleiotropic syndrome of dehydrated hereditary stomatocytosis, pseudohyperkalemia, and perinatal edema maps to 16q23-q24. *Blood.* 2000;96(7):2599-2605.
16. Beaurain G, Mathieu F, Grootenboer S, et al. Dehydrated hereditary stomatocytosis mimicking familial hyperkalaemic hypertension: clinical and genetic investigation. *Eur J Haematol.* 2007;78(3): 253-259.
17. Houston BL, Zelinski T, Israels SJ, et al. Refinement of the hereditary xerocytosis locus on chromosome 16q in a large Canadian kindred. *Blood Cells Mol Dis.* 2011;47(4):226-231.
18. Zarychanski R, Schulz VP, Houston BL, et al. Mutations in the mechanotransduction protein PIEZO1 are associated with hereditary xerocytosis. *Blood.* 2012;120(9):1908-1915.
19. Stewart GW, Corrall RJ, Fyffe JA, Stockdill G, Strong JA. Familial pseudohyperkalaemia. A new syndrome. *Lancet.* 1979;2(8135):175-177.
20. Iolascon A, Stewart GW, Ajetunmobi JF, et al. Familial pseudohyperkalemia maps to the same locus as dehydrated hereditary stomatocytosis (hereditary xerocytosis). *Blood.* 1999;93(9): 3120-3123.
21. Basu AP, Carey P, Cynober T, et al. Dehydrated hereditary stomatocytosis with transient perinatal ascites. *Arch Dis Child Fetal Neonatal Ed.* 2003; 88(5):F438-F439.
22. Vicente-Gutiérrez MP, Castelló-Almazán I, Salvía-Roiges MD, et al. Nonimmune hydrops fetalis due to congenital xerocytosis. *J Perinatol.* 2005;25(1):63-65.
23. Ami O, Picone O, Garçon L, et al. First-trimester nuchal abnormalities secondary to dehydrated hereditary stomatocytosis. *Prenat Diagn.* 2009; 29(11):1071-1074.
24. Li H, Handsaker B, Wysoker A, et al. The Sequence Alignment/Map format and SAMtools. *Bioinformatics.* 2009;25(16):2078-2079.
25. McKenna A, Hanna M, Banks E, et al. The Genome Analysis Toolkit: a MapReduce framework for analyzing next-generation DNA sequencing data. *Genome Res.* 2010;20(9): 1297-1303.
26. Schwarz JM, Rödelsperger C, Schuelke M, Seelow D. MutationTaster evaluates disease-causing potential of sequence alterations. *Nat Methods.* 2010;7(8):575-576.
27. Adzhubei IA, Schmidt S, Peshkin L, et al. A method and server for predicting damaging missense mutations. *Nat Methods.* 2010;7(4): 248-249.
28. Ng PC, Henikoff S. Predicting the effects of amino acid substitutions on protein function. *Annu Rev Genomics Hum Genet.* 2006;7:61-80.
29. Robinson JT, Thorvaldsdóttir H, Winckler W, et al. Integrative genomics viewer. *Nat Biotechnol.* 2011;29(1):24-26.
30. Chomczynski P, Sacchi N. Single-step method of RNA isolation by acid guanidinium thiocyanate-phenol-chloroform extraction. *Anal Biochem.* 1987;162(1):156-159.
31. Gibon J, Tu P, Bohic S, et al. The over-expression of TRPC6 channels in HEK-293 cells favours the intracellular accumulation of zinc. *Biochim Biophys Acta.* 2011;1808(12): 2807-2818.
32. De Franceschi L, Ronzoni L, Cappellini MD, et al. K-CL co-transport plays an important role in normal and beta thalassemic erythropoiesis. *Haematologica.* 2007;92(10):1319-1326.
33. Su W, Shmukler BE, Chernova MN, et al. Mouse K-Cl cotransporter KCC1: cloning, mapping, pathological expression, and functional regulation. *Am J Physiol.* 1999; 277(5 Pt 1):C899-C912.
34. Flatt JF, Guizouarn H, Burton NM, et al. Stomatin-deficient cryohydrocytosis results from mutations in SLC2A1: a novel form of GLUT1 deficiency syndrome. *Blood.* 2011; 118(19):5267-5277.
35. Vandorpe DH, Shmukler BE, Jiang L, et al. cDNA cloning and functional characterization of the mouse Ca2+-gated K+ channel, mIK1. Roles in regulatory volume decrease and erythroid differentiation. *J Biol Chem.* 1998;273(34): 21542-21553.
36. Nagase T, Seki N, Ishikawa K, et al. Prediction of the coding sequences of unidentified human genes. VI. The coding sequences of 80 new genes (KIAA0201-KIAA0280) deduced by analysis of cDNA clones from cell line KG-1 and brain. *DNA Res.* 1996;3(5):321-329, 341-354.
37. Satoh K, Hata M, Takahara S, et al. A novel membrane protein, encoded by the gene covering KIAA0233, is transcriptionally induced in senile plaque-associated astrocytes. *Brain Res.* 2006; 1108(1):19-27.
38. McHugh BJ, Buttery R, Lad Y, Banks S, Haslett C, Sethi T. Integrin activation by Fam38A uses a novel mechanism of R-Ras targeting to the endoplasmic reticulum. *J Cell Sci.* 2010;123(Pt 1): 51-61.
39. Coste B, Mathur J, Schmidt M, et al. Piezo1 and Piezo2 are essential components of distinct mechanically activated cation channels. *Science.* 2010;330(6000):55-60.
40. Gottlieb PA, Bae C, Sachs F. Gating the mechanical channel Piezo1: a comparison between whole-cell and patch recording. *Channels (Austin).* 2012;6(4):282-289.
41. Gottlieb PA, Sachs F. Piezo1: properties of a cation selective mechanical channel. *Channels (Austin).* 2012;6(4):214-219.
42. Bae C, Sachs F, Gottlieb PA. The mechanosensitive ion channel Piezo1 is inhibited by the peptide GsMTx4. *Biochemistry.* 2011; 50(29):6295-6300.
43. Kim SE, Coste B, Chadha A, Cook B, Patapoutian A. The role of Drosophila Piezo in mechanical nociception. *Nature.* 2012;483(7388):209-212.
44. Wollscheid B, Bausch-Fluck D, Henderson C, et al. Mass-spectrometric identification and relative quantification of N-linked cell surface glycoproteins. *Nat Biotechnol.* 2009;27(4): 378-386.
45. Choudhary C, Kumar C, Gnad F, et al. Lysine acetylation targets protein complexes and co-regulates major cellular functions. *Science.* 2009;325(5942):834-840.
46. Olsen JV, Vermeulen M, Santamaria A, et al. Quantitative phosphoproteomics reveals widespread full phosphorylation site occupancy during mitosis. *Sci Signal.* 2010;3(104):ra3.
47. Dubin AE, Schmidt M, Mathur J, et al. Inflammatory signals enhance piezo2-mediated mechanosensitive currents. *Cell Rep.* 2012;2(3): 511-517.
48. Pasini EM, Kirkegaard M, Mortensen P, Lutz HU, Thomas AW, Mann M. In-depth analysis of the membrane and cytosolic proteome of red blood cells. *Blood.* 2006;108(3):791-801.